Design of Distributed Mail-slot Propulsion System on a Hybrid Wingbody Aircraft

ByungJoon Lee[1], and May-Fun Liou[2], Hyoungjin Kim[3]

NASA Glenn Research Center, Cleveland, Ohio, 44135

Abstract

This paper deals with designing a thrust distribution strategy when a Turboelectric Distributed Propulsion (TeDP) system of 16 embedded propulsors is installed on an aerodynamically optimized hybrid wing-body configuration. This HWB previously designed to satisfy conditions of trim, longitudinally static stability and specific cargo space is employed as the baseline configuration for the current study of seeking an optimal propulsion/power system. According to the nature of the entrance flow condition for each distributed propulsion passage in hybrid wing-body aircraft, the ingested boundary layer thickness differs and results in different propulsive reaction. An optimal distribution of thrust and power output is determined by how the system utilizes the propulsive characteristics of each passage. The design space and the number of design variables are selected and described accordingly. An actuator disk model is employed to model thrust generation and shaft power from the propulsor. To carry out the optimization of the propulsion/power system on a computationally expensive CFD model, a Kriging method in conjunction with a Genetic Algorithm (GA) is applied. Throughout the design process, the propulsion performances of the sampled propulsion/power system are analyzed and compared to those of a clean flow engine. Besides the thrust and shaft power, the performance metrics includes mass flow rate, fan pressure ratio, propulsive efficiency, and flow distortion. Minimization of total shaft power from the distributed engine is performed at multiple thrust levels. The benefit of boundary layer ingestion propulsion system is quantified via comparison of thrust equivalent, shaft power and mass flow equivalent clean flow engines with CFD based system design.

Nomenclature

α	= Angle of incidence	ADP	= Aerodynamic Design Point
ρ	= Density	DPCP	= Distortion index
C_D	= Drag coefficient	FPR	= Fan Pressure Ratio
C_P	= Specific heat capacity	MFR	= Mass Flow Rate
C_t	= Thrust coefficient	N_c	= Fan shaft speed
$\dot{m}$	= Mass flow rate	T	= Thrust
S_{ref}	= Reference area	OGV	= Outlet Guide Vane
T_s	= Static temperature	PAI	= Propulsion Airframe Integration
p_s	= Static pressure	TeDP	= Turboelectric Distributed Propulsion
A	= Area	x	= Axial direction
Subscript		i	= index of slot thruster
b	= baseline	∞	= free stream
0	= target	*total*	= summation of *I* from 1 to 8

I. Introduction

A hybrid wingbody (HWB) concept is being considered by NASA as a potential subsonic transport aircraft that meets aerodynamic, fuel, emission, and noise goals in the time frame beyond the 2050. While the concept promises advantages over conventional wing-and-tube aircraft, it poses unknowns and risks, thus requires in- th and broad assessments. Specifically, the configuration entails a tight integration of the airframe and propulsion geometries; the aerodynamic impact has to be carefully evaluated. This realization has led to several studies and research efforts in the past, including a system analysis[1] of a baseline design of the N3-X, high-fidelity flow simulations to understand the effects of the propulsion-airframe integration (PAI) on the flow and later aerodynamic redesign through optimization techniques. Among those efforts, HWB has been dealt in three prospects: airframe with nacelle, propulsor with flowpath, and PAI with stability. On the airframe/nacelle side, a CAD (Computer-Aided Design)-free shape parameterization, the Class function/Shape function Transformation (CST) which is a non-dimensional airfoil/wing generation method, was adopted to effectively construct the HWB airframe-propulsion configuration[2]. This

[1] *Vantage Partners, LLC*, Aerospace Engineer, Turbomachinery and Turboelectric Systems Branch. Senior Member AIAA
[2] Aerospace Engineer, Inlets and Nozzles Branch. Senior Member AIAA
[3] *Vantage Partners, LLC*, Aerospace Engineer, Senior Member AIAA; currently a Professor at Kyung Hee University, Republic of Korea.

parameterization enables a PAI design approach that considered both the airframe and propulsion systems together at the outset of aerodynamic design of the aircraft. Furthermore, the nacelle cowl shape was designed and optimized using adjoint method to improve aerodynamic performance of the nacelle[3]. On the propulsion side, an efficient body force approach was suggested to incorporate the effects of turning and flow loss from the fan stage[4,5] to make the PAI optimization computationally feasible. Recently, aerodynamic shape design and optimizations were performed to determine geometric shape parameters by minimizing the drag while subject to the lift, pitching moment, and cargo constraints[6]. Thus, a conceptual configuration of the N3-X aircraft for 300-passenger-seats was designed and named N3X-DEP300 (DEP: distributed electric propulsion). The work resolved the challenges against minimal drag with fixed lift, being longitudinally static stable, trimmable with physical space cargo, but the internal flowpath of the propulsor was not modeled by assuming a uniform back pressure boundary condition at the inlet throat. However, the accuracy of this assumption may not be adequate for highly distorted flows at fan faces due to a significant numerical flow blockage effect. Thus, an actuator disk model is applied in the present study for modeling the suction effect of fan operation in higher fidelity. .

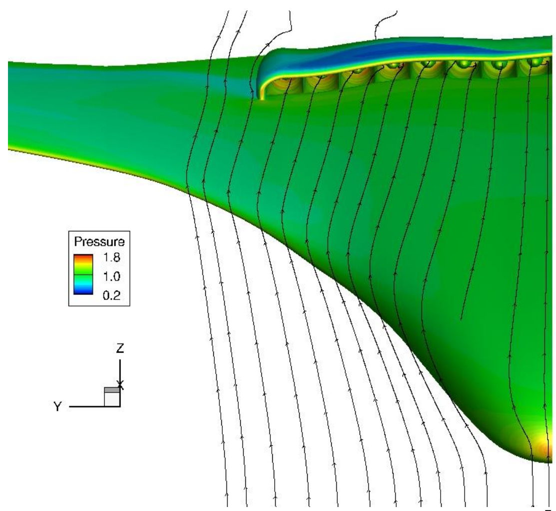

Figure 1. Previous result of the Navier-Stokes simulation of the N3-X[5]; there are 8 mail-slot fan-propulsors installed on each side from the symmetric plane : surface pressure contours and streamlines [5].

A propulsion system using 16 distributed electric fans in the mail-slot propulsor, proposed by the system analysis[1], was analyzed in Ref. 5. High-fidelity RANS simulations employing a body force model were conducted to account for the inlet-fan interaction. The embedded propulsor takes the boundary layer ingestion (BLI) at the inlet. Though the BLI inlet has several merits: reduced structural weight and noise, and improved propulsive efficiency by reducing form drag and wetted area, it also has shortcomings related to the performance and operability of the propulsor such as high flow distortion and low pressure recovery[8.9]. It is expected that the distortion at the fan face varies with the physical location of the propulsor installed on the airframe. Overall flow features around the configuration is visualized by the surface pressure contours and streamlines into the nacelle in Fig. 1. It shows the airframe and the embedded nacelle are strongly coupled and the aerodynamic performance tightly interacts with BLI propulsion system which was also pointed out later in Ref. 10.

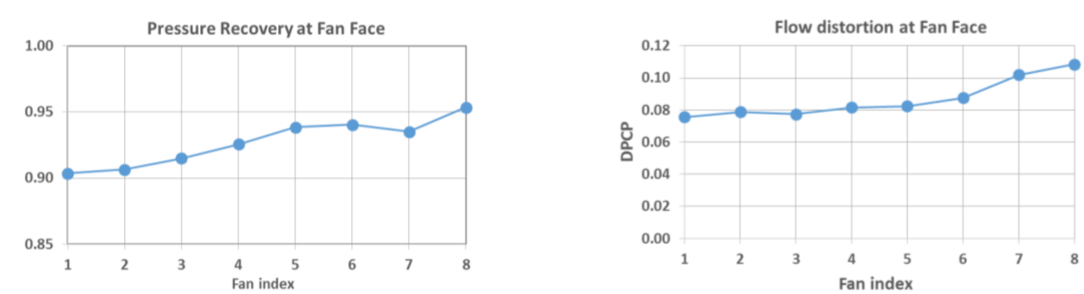

(a) Total pressure recovery at fan face **(b) Distortion index DPCP at fan face**

Figure 2: Previous results of flow characters at fan faces of eight passage at half span of the N3-X [5].

Figures 2-(a) and (b) compare flow quality metrics related to the propulsion system such as fan-face pressure recovery and distortion index DPCP of the eight passages of the baseline N3-X configuration. Here, the fan index denotes the numbered slot counting from the center to the tip of the wing span. The pressure recovery increases from inboard to outboard. This is because the thickness of the boundary layer ingested into each inlet increases as it goes outboard. The fan performance of an embedded nacelle will generally be degraded due to the flow distortion at the inlet relative to an isolated fan subject to a uniform inflow condition. In case of the distributed mail-slot nacelle of N3-X, the inlet flow condition of each passage differs as the thickness of the incoming boundary layer differs subject to the airfoil shape of the corresponding section of fuselage. The reaction of the fan blades subject to evenly distributed rotational speed in uniformly sized slots are presented in Figs. 3-(a) and (b). Figure 3-(a) shows that the mass flow rate increases and fan pressure ratio decreases as it goes outboard, which is again attributed to the characteristics of the ingested boundary layer. Smith[11] listed those characteristics of the inlet boundary layer including shape factor, pseudo energy factor, and the inlet performance such as the flow distortion and pressure recovery, and mass flow rate. Shown in Fig. 3-(b) are the thrust force and shaft power, which also are functions of the characteristics of the inlet boundary. Similarly, Figures 4-(a), and (b) present the normalized total pressure contours at fan face planes for passages 1 and 8, respectively. In N3-X, slot propulsor ingests more clean flow as the boundary layer gets thinner toward the outboard. As a result, the passage 1 contains a horizontally layered variation of the total pressure, which also implies that the profile at the inlet is layered in a similar manner. Its inlet boundary layer is the thickest among all 8 slot propulsors. On the other hand, the passage 8 shows asymmetric contours of total pressure due to significant side-wind components of the inflow. This study resulted in a new design of the installed nacelle by moving the propulsion system about 4% downstream along the root line and demonstrated a significantly reduced degradation in performance. This trend suggests that each propulsor despite arranged in an array may need to be designed individually to maximize the fuel burn saving from BLI for a thrust requirement.

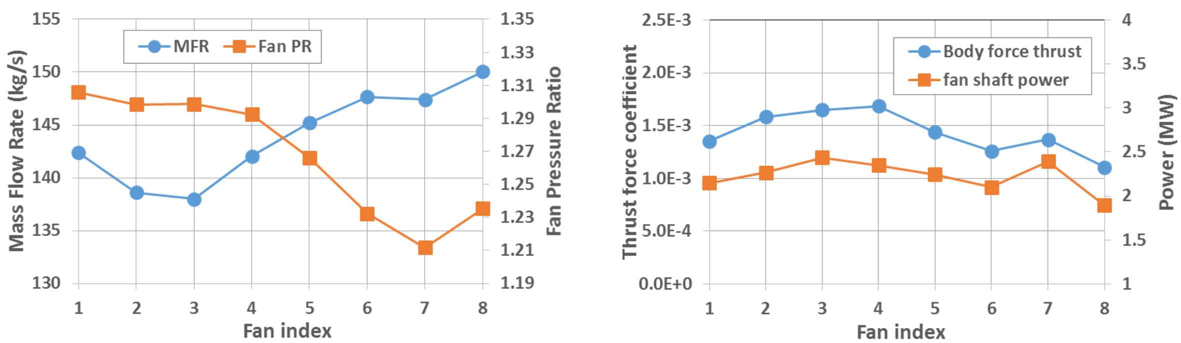

(a) Mass flow rate (corrected flow) and fan pressure ratio **(b) Thrust and shaft power**

Figure 3: Previous results of the installed fan performance of 8 passages at half span of N3-X [5].

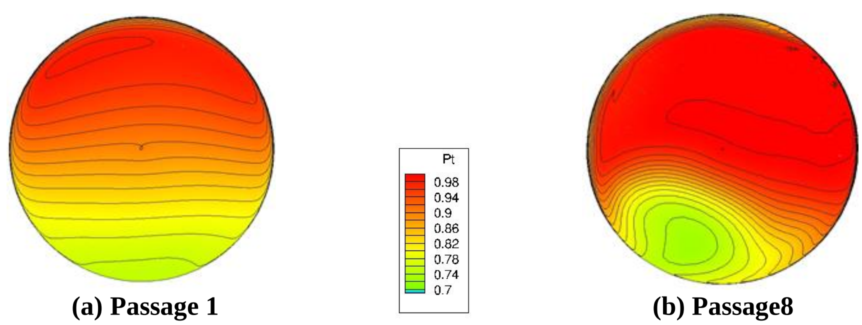

(a) Passage 1 **(b) Passage8**

Fig. 4 Previous results of the distortion at fan face indicated by total pressure contours of passage 1 and 8.

In the following sections, section II describes the aerodynamic design of the baseline propulsor. Starting with parameterization of the mail-slot propulsor, it addresses a design principle based on the area rule regarding the designs of the inlet, flowpath and nozzle. PAI CFD results of the baseline propulsor with N3X-DEP300 [6] are provided and its propulsive performance is evaluated accordingly. In addition, an equivalent size clean flow engine, i.e. free of boundary layer at inlet, is analyzed for comparison. In section III, the objective of the optimization, design processes are described. Furthermore, the critical factors of the propulsor design for a single passage toward minimization of required shaft power are discussed through the cases from Latin Hyper cube sampling and an ideal thrust distribution is studied through design of experiment. The external shaping of the airframe and nacelle from the previous PAI design work is adopted.[6]

II. Assessment of Baseline Configuration

A. Nacelle Geometry and Flowpath Parameters

Each of the multi-slot propulsors consists of the inlet with shaped-duct, electric propulsors, center-body, nozzle and the resulted internal flowpath. For a flexible geometric representation, NURBS/B-spline based parameterization is used to generate the flowpath as shown in Fig. 5. Figure 5 lists all the parameters of the propulsor in schematic way. The orders of B-Splines from stations 0 to 5 respectively can be simply adjusted per the input by the designer. Figure 6 shows the HWB configuration with an array of 16 propulsors installed on the upper surface deployed across the spanwise direction. The fan diameter is 1.02, inlet captured area (A_c) is 0.72m^2 and nozzle throat area is 0.6m^2.The inlet area ratio is 1.17.

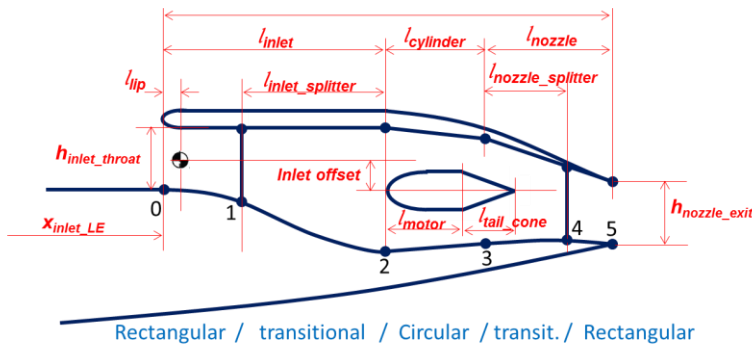

Figure 5. Schematic representation of the mail-slot propulsor parameterization of a single passage mail-slot propulsor.

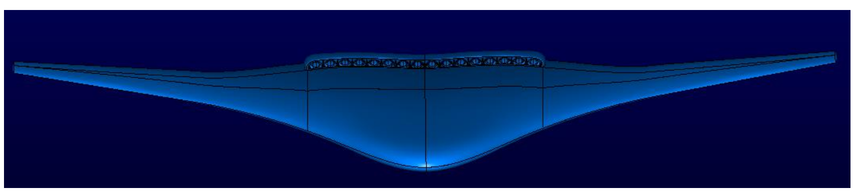

(a) Mail slot nacelle installed on the N3X-DEP300

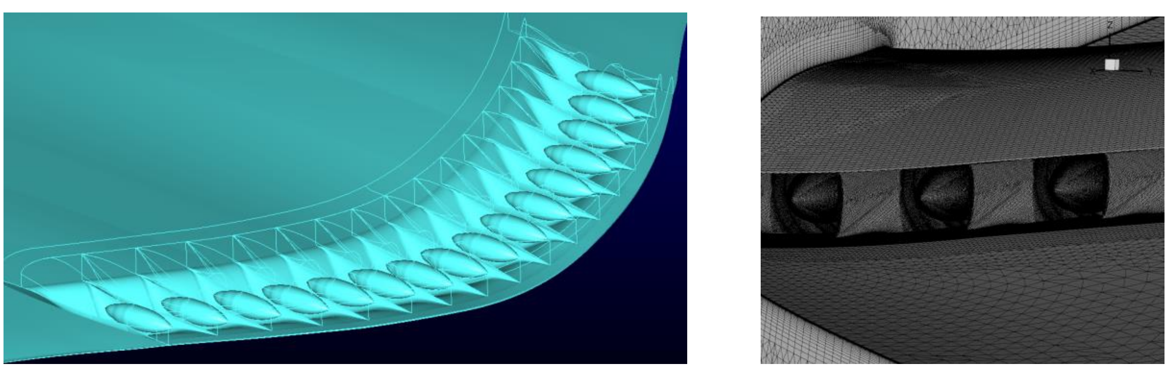

(b) Internal surface of mail-slots (Left) and the computational mesh near nozzle exit (Right)

Figure 6. N3–X DEP300 configuration with installed mail-slot propulsors

To avoid choking throughout the duct, the cross sectional area of the flowpath is monotonically diverging from the inlet to the aerodynamic interface plane (AIP, station 2 as indicated in Fig. 5). Also the contraction from AIP to the nozzle plane (station 4) is controlled by area rule to keep the flow accelerated to Mach number of 0.95 at the design point (ADP). Figure 7 compares the cross-sectional area distribution of the original N3X slot design and new slot for N3X-DEP300 along the axial direction, x. The figure shows that the modified duct area allows a benign diffusion between stations 1 and 2 and flow acceleration through station 2 and 3. After implementing the modified flowpath into the airframe, a baseline CFD analysis is performed to investigate the performance of the propulsors. The center body is from a scaled flowpath of GE R4 fan and an actuator disk model is used to model thrust generation and shaft power from the propulsor. The actuator disk model is located at the fan face which is about 0.2 m downstream of the AIP station. The hub to tip radius ratio of the fan face is 0.3.

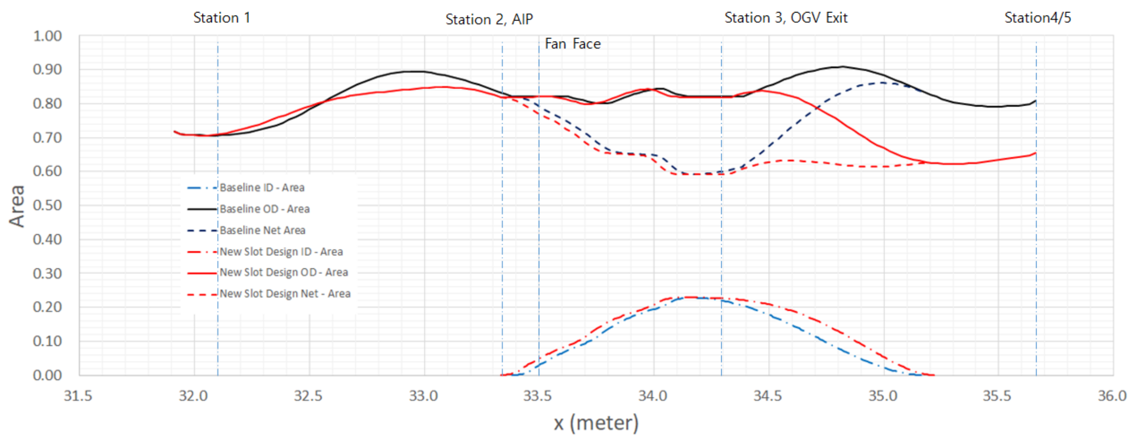

Figure 7. Area rule of mail-slot passage

B. CFD analysis of Baseline Configuration

The flow solver FUN3D which is a suite of codes for flow analysis, design and optimization is employed[13] here. It uses mixed-element unstructured grids in a various formats, including structured multi-block and overset grid systems. Its one-equation Spalart-Allmaras turbulence model was chosen for its performance in dealing with external flow. FUN3D has different levels of model to simulate a rotating blade system. Among the available options, the time-averaged actuator disk method is adopted. There is no need to build the computational grids for the rotating blades, since it utilizes momentum/energy source terms to represent the influence of the rotating blade system. Hence, the computation and grid generation are simplified. The load on the rotor is assumed to have a constant total pressure rise over the disk. The pressure rise is determined by thrust coefficients (C_t) in the input file. The definition of the thrust coefficient is as described in Eq. (1)

$$C_t = T/\left(\rho \pi R^2 V_{tip}^2\right) \tag{1}$$

Where T denotes the thrust, ρ represents the density of the inlet flow, R is radius of rotor blade and V_{tip} is tip speed.

The conditions of the CFD analysis of the PAI modeling is that the free stream Mach number is 0.84, Reynolds number of 7.2mil. per unit length (m). Angle of attack is 3.06 per longitudinal stability analysis for trim condition.[6] The baseline analysis is carried out through various thrust coefficients case to estimate that power and thrust could be obtained at the cruise condition at 40kft. Altitude. The input thrust coefficients for all 16 mail-slots are uniform.

Furthermore, the performance of a same size clean flow engine is analyzed with at the same condition as a reference to investigate the power saving of BLI engines. Here, the impact of boundary layer ingestion is not considered so that the reactions of thruster such as the fan pressure ratio, thrust and shaft power estimated by the thrust coefficient show non-linear tendency in the present study.

CFD analyses over the PAI configuration with different C_t are conducted to investigate the sensitivity of upstream potential flow field over the fuselage with respect to the fan pressure ratio as shown in Figs. 8. The surface pressure contours from different C_t show marginal differences between C_t=0.14 and C_t=0.26, but the border of the yellow zone (Ps/P_∞=0.65) in C_t=0.26 case starts deviating from others. This is an indication of the captured area ratio of the inlet starts exceeding full-flow (A_0/A_c=1.0). Also it is noted that the leading edge of the wing at 50% span expands more as C_t increases meaning that there is more side slip to the nacelle as the mass flow is ingested into the nacelle. An example of the thrust against shaft power for the "thrust coefficient sweep" is shown in Fig. 9. Figure 9 presents the required shaft power relative to the total net thrust out of 16 slots of the baseline propulsor and clean flow engine. At the cruise condition which is indicated by a black dashed line, BLI engine outperforms the clean flow one. BLI engines, however, tend to reach the choking conditions earlier than the clean flow engine, thus, the power saving benefits gets smaller as the higher thrust is generated. This is because the flow blockage of low momentum boundary layer flow, in other words, low mass flow stream takes most of duct volume. As a result, the effective duct area is smaller relative to the clean flow engine. This phenomenon can be interpreted as the fact that lower fan pressure ratio, or wider fan diameter than clean flow engine are favorable to maximize the benefit of the boundary layer ingestion for a same mass flow rate condition.

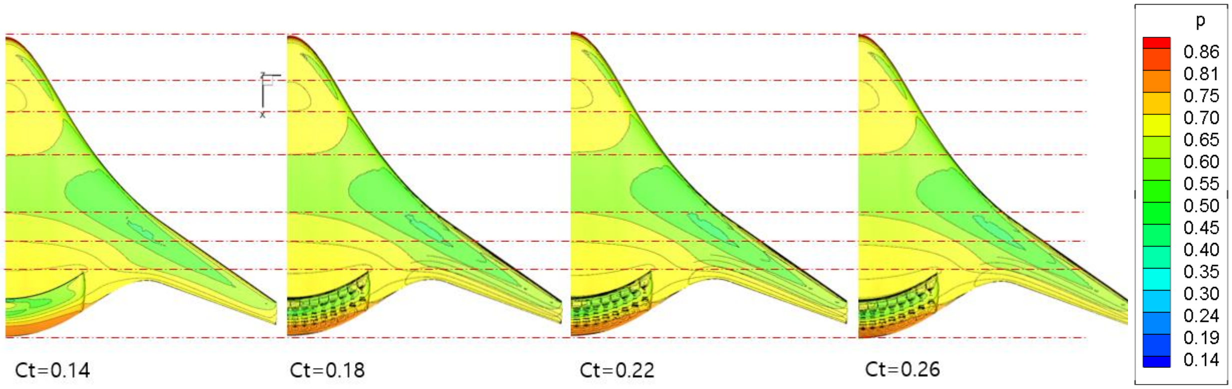

Figure 8. Comparison of surface pressure distribution (upper surface) with respect to different fan pressure ratio. (pressure level is normalized to the freestream pressure p_∞)

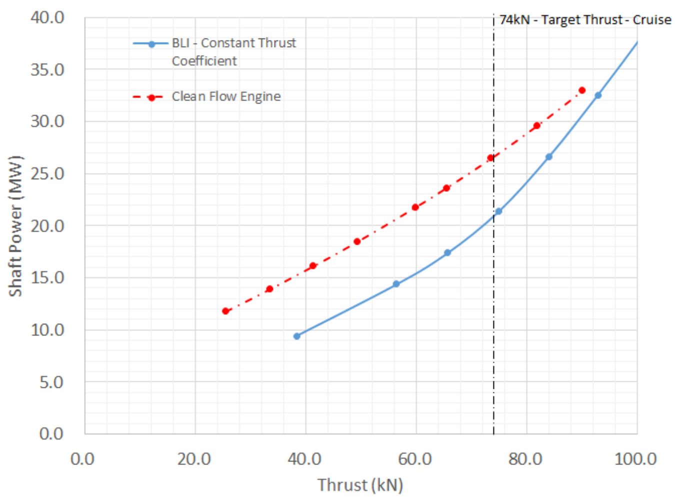

Figure 9. Comparison of shaft power curves relative to total net thrust, BLI vs Clean Flow Engine

C. Benefits of BLI propulsion system.

Figure 10 compares thrust generation from 16 slots of the BLI thruster and 12 slots of clean flow engines. The number of slots of the clean flow engine is set to match the shaft power with that of the 16 BLI slots. Thus, the area of fan face of the BLI engine is 1.33 times larger than the clean flow engine. At a same mass flow rate conditions, the BLI mail-slot thruster generates about 20kN more thrust than clean flow engines do. Furthermore, the difference of thrust increases at lower mass flow rate conditions, i.e., lower power conditions. Figures 11 compares the total pressure contour of select BLI slots (slot 1 and 8) and a clean flow engine at total net thrust of 74kN for 16 slots, i.e., 4.625kN/slot. Fan pressure ratio (FPR) is 1.27 for both cases. Thus, BLI could achieve same pressure ratio with lower thrust coefficient input, i.e., less shaft power is required compared with the clean flow engine because of lower mass flow rate and ram drag.

D. Baseline - Constant Thrust Coefficient Cases

For the baseline cases, a constant thrust coefficient is assigned for all the slots evenly meeting the output thrust with the requirement. The CFD analysis data correlates thrust coefficients with total thrust (in averaged value per slot, 1/16T0) and local thrust of each slot as presented in Fig. 11. It is notable that low thrust case around 40kN shows only about 0.2kN variation among the slots, while high thrust case (111kN) shows a significant difference about 0.8kN. This fact explains the reason that BLI engine loses the power saving benefit as the thrust gets higher as observed in Fig. 9. Figures 13 and 14 show the total pressure contours at AIP and OGV exits of Ct=0.14, Ct=0.26 to compare the characteristics of propulsor at high and low thrust conditions, respectively. A thrust equivalent clean flow engine cases are plotted in the same figures. As observed in the AIP contours both low and high thrust cases, there are not much difference between the inboard and outboard slots in terms of the height of boundary layer ingestion while the original N3X shows a significant difference between slot 1 and slot 8 contours as shown in Figs. 4. Furthermore, the constraint for cargo space increased the wet area of fuselage in N3X-DEP300 PAI configuration, especially, fuselage chord length at the upstream of outboard slots increased in the planform layout. The airfoil thickness constraint – also to accommodate the cargo – increased more as well. As a result, the ingested boundary layer is much thicker than the original configuration. This change helped the performance in terms of propulsion system. The performance of the baseline mail-slot might be already close to a maximum power saving of BLI at low thrust conditions. Thus, the focus of the present design is placed on high thrust condition where the inboard BLI slots starts choking near T_0=80kN and higher.

A surrogate model will be built from the sample points and is coupled with a genetic algorithm for the total shaft power minimization subject to a constraint of a target thrust, T_0. The design process for the optimal distribution of the thrust across the mail-slots will be described in the following section.

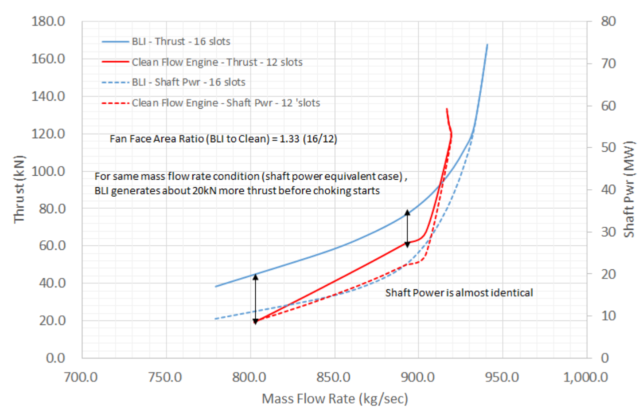

Figure 10. Thrust comparison at shaft power equivalent case - fan face area ratio (BLI to Clean) = 1.33.

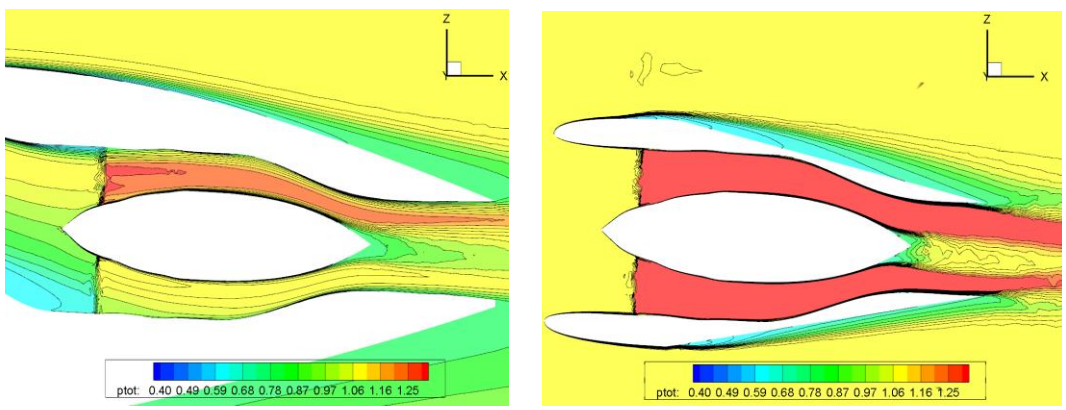

(a) Slot 1 – BLI engine (Ct=0.20) **(b) Clean Flow Engine (Ct=0.26)**

Figure 11. Comparison of total pressure contours of thrust equivalent cases

(Note that the internal flowpath of the clean flow engine from AIP to the nozzle exit is identical to a BLI slot, the external nacelle is drawn by an arbitrary line which does not affect the internal flow pattern at station 2 and 3, where the net thrust and shaft power are measured.)

III. Design Optimization

A Turboelectric Distributed Propulsion (TeDP) system which consists of two superconducting generators, superconducting electrical transmission lines, and an array of superconducting motor driven fan was proposed in the system study.[1] The distributed propulsors are embedded in continuous nacelles on the upper fuselage surface near trailing edge. These two superconducting generators are driven by two tip-mounted turboshaft engines. The distributed electric fans are driven by the power generated by the turbo-generators. The system level requirements and constraints of both the propulsion and electrical performance with optional cooling systems at cruise condition from Ref. 1 are summarized in table 1. The thrust requirement is 74kN at 40k feet altitude and the power requirement for the propulsion system is 16.7MW. The maximum power available for the electric system of the whole aircraft is 30MW including the propulsion.

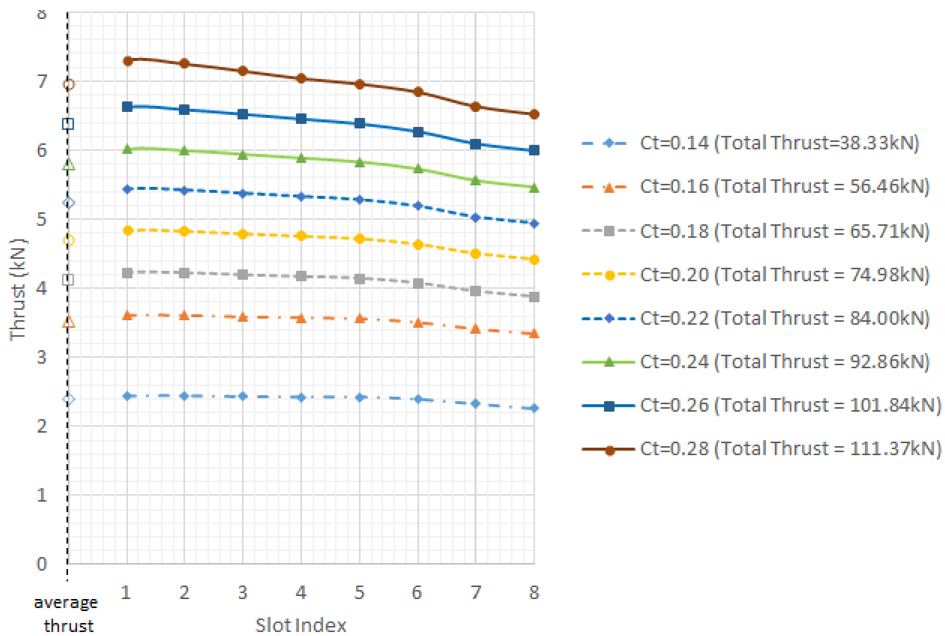

Figure 12. Thrust generation for each slot per constant thrust coefficient.

Cruise Operating Conditions	P (kW)		T (kN)		FPR
	16695		74		1.3
	M_∞	**Temp** (°R)	**Re/m**	**Alt.(kft.)**	**AOA**
	0.84	389.97	7.2 mil.	40	3.0

Table 1. System Design Requirements [1]

The present study bases off a new PAI configuration[6], N3X-DEP300, of which the chord length at the wing root is 36 m while that of the original N3X is 41 m. However, the reference area, S_{ref} increased from 427.7m^2 to 467.2 m^2 as the cargo space for 300 passenger seats is incorporated in the planform layout. Per the author's previous study[6], the PAI configuration has about 35% more pressure drag relative to the clean wing configuration as the thrust estimation in the Ref. 1 is performed with the clean wing configuration of the original N3-X. The airframe design optimization reduced the aerodynamic drag by 20%. As a result, the thrust requirement in the present study is targeted at 80kN which is deviated from the system analyses for the first design of N3-X. As shown in Fig. 8, the target thrust requires almost 24MW of shaft power which would leave 6MW for other electric systems and the battery charge.

In response to the required net thrust and shaft power of the operation of the TeDP system, a scheme is devised to seek after the optimized thrust distribution among the 16 mail-slot propulsors minimizing the required shaft power. . In general, the CFD based aerodynamic design requires a prohibitive cost relative to other disciplines in a MDAO (multi-disciplinary analysis and optimization) environment, thus not popularly used at the system level design because it demands heavy computations in routine tasks such as design optimization, design space exploration, sensitivity analysis etc. The cost problem of CFD is even much more significant in case of distributed propulsion system. Thus, instead of a direct design, a design of experiment using surrogate model is applied to the current optimization process.

If a surrogate model is dedicated to the aerodynamic analysis, the system design process can save lots of cost without degrading the fidelity of performance prediction.

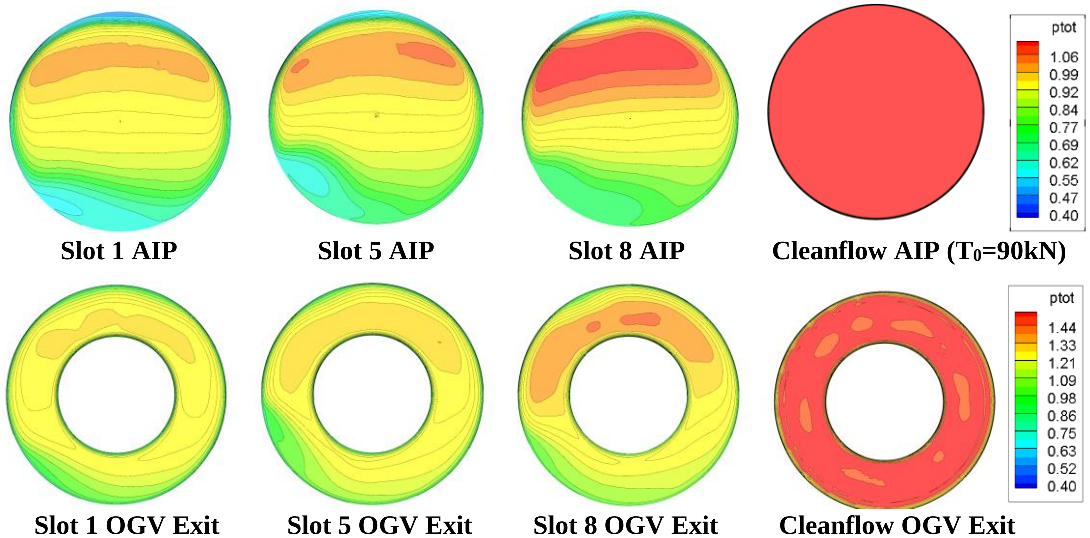

Figure 13.Total pressure contours at T_0=100kN (Ct=0.26)

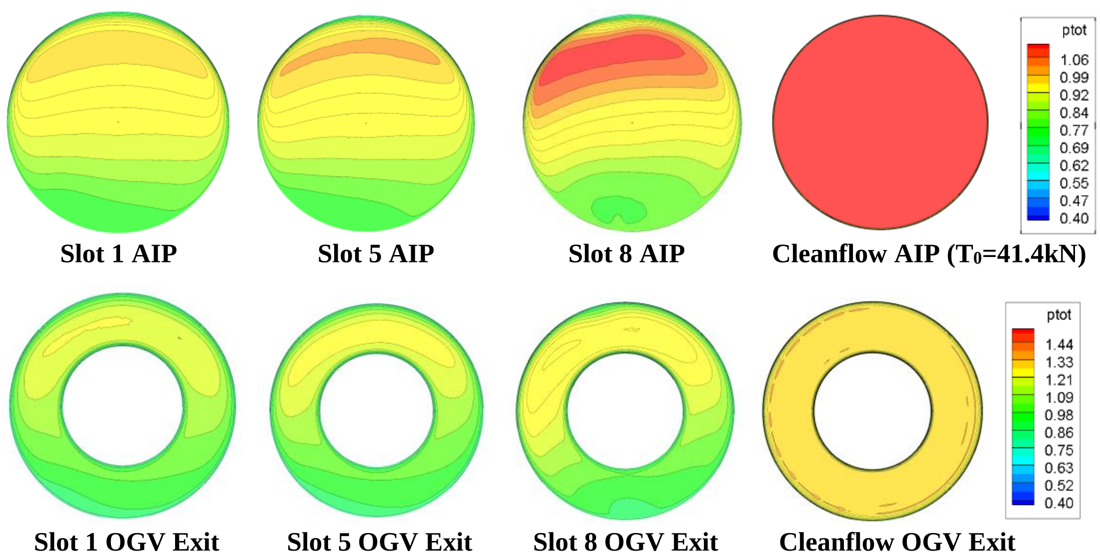

Figure 14.Total pressure contours at T_0=47.4kN (Ct=0.14)

A. Objective Function

The objective for this optimization is to find an optimal thrust distribution with minimum shaft power required. Thus, the definition of objective function is as follows;

$$\text{Minimize} \quad \boldsymbol{P} = 2 \times \{\textstyle\sum_{i=1}^{8} P_i\}, \tag{2}$$

$$\text{Subject to} \quad (T_{total} - T_0) \geq 0.0,\ T_{total} = 2 \times \textstyle\sum_{i=1}^{8} T_i \tag{3}$$

The thrust and shaft power are measured between station 2 and 3 in Fig. 7. The thrust is the difference of momentum and pressure flux between the stations as described in Eq. (4).

$$T_i = \int_{A_{i,3}} (\rho V_x |\vec{V}| + p_s - p_\infty) dA_z - \int_{A_{i,2}} (\rho V_x |\vec{V}| + p_s - p_\infty) dA_z\,, \tag{4}$$

where p_∞ is the ambient pressure. The shaft power is calculated by the total energy difference as defined in Eq. (5)

$$P_i = \int_{A_{i,3}} \rho V_x \left(\frac{1}{2}\left|\vec{V}\right|^2 + \frac{p_s}{\rho} + C_p T_s\right) dA_z \text{-} \int_{A_{i,2}} \rho V_x \left(\frac{1}{2}\left|\vec{V}\right|^2 + \frac{p_s}{\rho} + C_p T_s\right) dA_z \quad (5)$$

B. Surrogate Model

As a demonstration of the above idea to apply surrogate models in the system level design, the net thrust and shaft power of 8 mail-slot propulsors (half domain) with respect to the thrust coefficient input per slot are substituted by a kriging model[14,15]. NSGA-II[16] is employed to optimize the thrust distribution. Due to surrogate models are constructed using a data-driven, bottom-up approach, a fair sampling in the design space is critical to mimic the behavior of the cost functions versus the design parameters as closely as possible. The sampling method of Latin hypercube sampling (LHS) for statistically generating a near-random sample of parameter values from 0 to 1 in a multidimensional distribution is employed. In the present study, 80 random sample points for 8 thrust coefficients. Herein, 0.5 is set as the nominal thrust coefficient, 0.226, for each slot and 0 depicts -25%, while 1 represents +25% from the nominal value, i.e., 0.1695 and 0.2825 respectively. Figure 15 presents the shaft power curve relative to thrust of slot 1 and slot 8 from the sampling table. Slot 8 where the amount of the boundary layer ingestion is relatively smaller relative to other slots requires higher shaft power than slot 1does at low thrust condition. On the other side, the slot 1 starts losing the power saving benefit as the thrust gets higher so that it shows even worse performance than the clean flow engine at above 6.4kN.

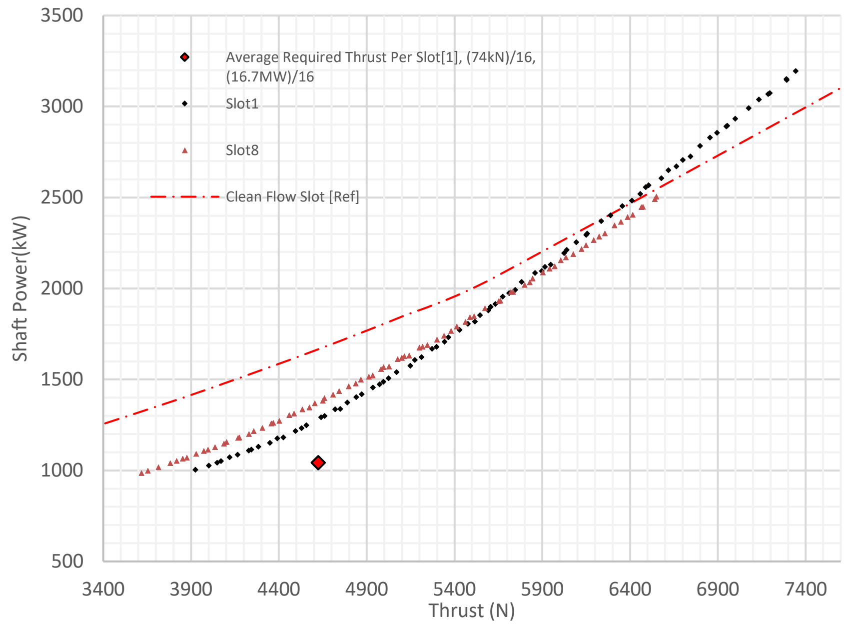

Figure 15. Shaft Power vs thrust coefficient of slots 1 and 8 from the sampling data.

C. Optimization for thrust distribution

The optimization is carried out for 6 different target thrust conditions at every 10kN between T_0=50kN~100kN to study the overall available performance capacity of the given mail-slots over wide range of operating conditions. The main target thrust is T_0=80kN as stated above. The history of the best individuals over 250 generation are for 80kN is presented in Fig.16. The population size per generation is 1000. The optimum solution reaches a convergence criteria after about 100 generations. The guideline for thruster design at each passage from the optimization is provided in Table 2. The point from the CFD analysis of the optimal distribution is within 0.5% error from the predicted value from the surrogate model. Figures 17 show the comparison of the performance metrics of 8 slots of the constant thrust coefficients case and optimized solution at 80kN. The thrust and shaft power distributions show a linear sensitivity to the fan pressure ratio distribution. The slots that ingest lower boundary layer amount at the outboard locations (slot 7 and 8) tend to operate at higher fan pressure ratio, thus, generating more thrust while the inboard slots that ingest more boundary layer tend to lower the fan pressure ratio to maximize the power saving. As a result, the optimized distribution at 80kN thrust case reduced the total shaft power from 24.307MW to 24.080MW (1% reduction). The power saving of the higher thrust case is more notable. The optimized distribution at 100kN reduces the power consumption from 38.926MW to 37.203MW (4.4% reduction). This is because the high thrust case has most of inboard BLI slots choked due to the flow blockage of boundary layer. Thus, re-distributing thrust based on the flow capacity relieved the extreme power consumption. However, the thrust is reduced from 101.836kN to 99.835kN at the same time. As a result, the actual reduction will be estimated by about 0.3MW based on the Figure 18. Figure. 18 shows the shaft power curve with respect to the thrust generation. It shows that baseline BLI has benefit of 0.6MW saving at 100kN relative to the clean flow engine and the optimal distribution of thrust delivers additional 0.3MW saving.

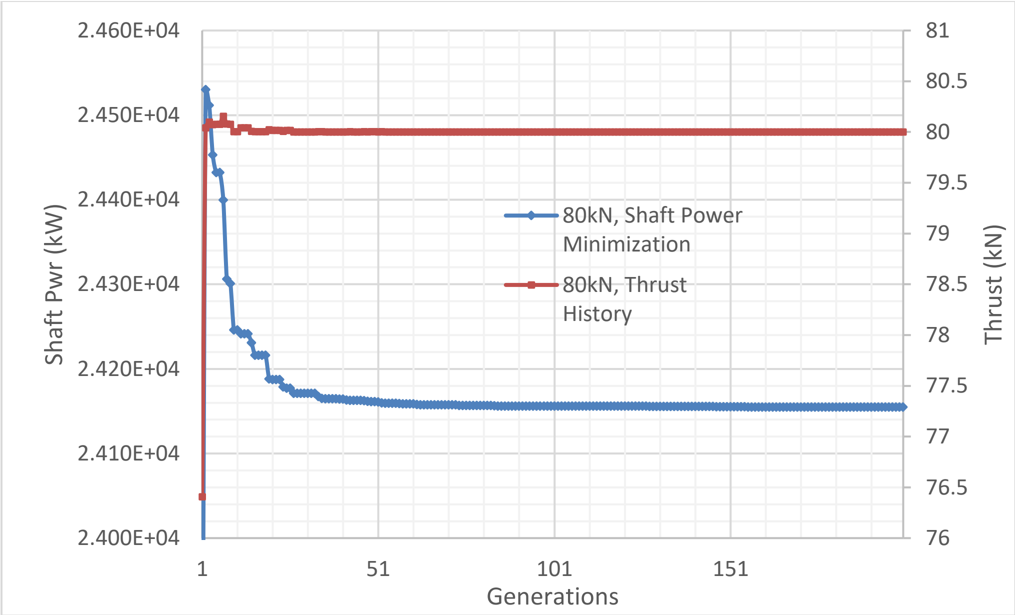

Figure 16. Convergence History of Shaft Power Minimization with Target Thrust at 80kN

	Slot 1	Slot 2	Slot 3	Slot 4	Slot 5	Slot 6	Slot 7	Slot 8
MFR (kg/sec)	55.07	55.18	55.77	55.88	55.92	56.53	57.30	56.95
FPR	1.278	1.280	1.284	1.279	1.287	1.288	1.306	1.306
Propulsive Efficiency	1.505	1.496	1.436	1.361	1.417	1.400	1.543	1.587
Distortion(%)	66.7	66.2	67.6	68.7	71.0	73.7	76.7	77.4
Thrust (kN)	4.759	4.839	4.946	4.868	5.016	5.017	5.325	5.273
Shaft Pwr (MW)	1.347	1.378	1.452	1.417	1.483	1.517	1.736	1.710

Table 2. Specification and Performance Requirements of Mail-slot Propulsors (T_0=80kN)

IV. Conclusions

A system design approach for a system of distributed electric propulsors for a new hybrid wing/body configuration, dubbed as the N3X-DEP300, is carried out via a surrogate model based design optimization. Minimization of the required shaft power subject to a target thrust of 80kN at cruise condition is performed. The performance of the BLI engine is evaluated in comparison with a thrust-equivalent clean flow engine, and a power equivalent (mass flow equivalent) clean flow engine. The distributed mail-slot BLI engine is demonstrated to save about 6MW power for the same thrust conditions (40kN~70kN). At high thrust conditions, the high BLI slots located inboard area start to choke earlier than clean flow engines, thus the power saving is reduced as the target thrust increases. However, an additional power saving about 0.4MW can be achieved by a novel thrust distribution strategy. The present paper successfully demonstrates that a system level high-fidelity design and optimization of the distributed BLI engines is feasible via CFD and surrogate model and high computational efficiency is still maintained.

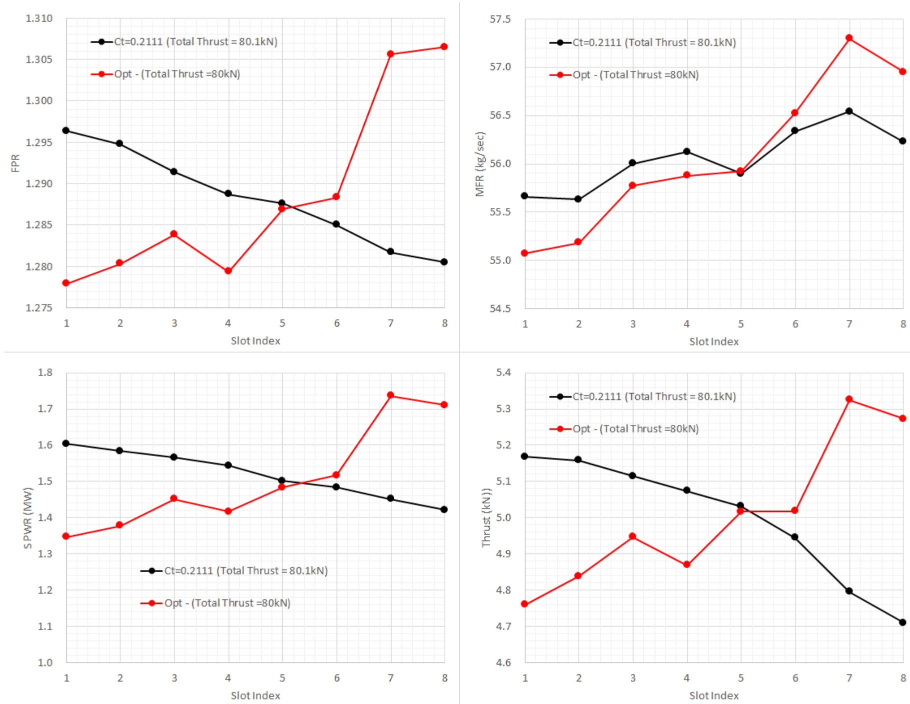

Figure 17. Performance comparison between constant thrust coefficient and optimized distribution

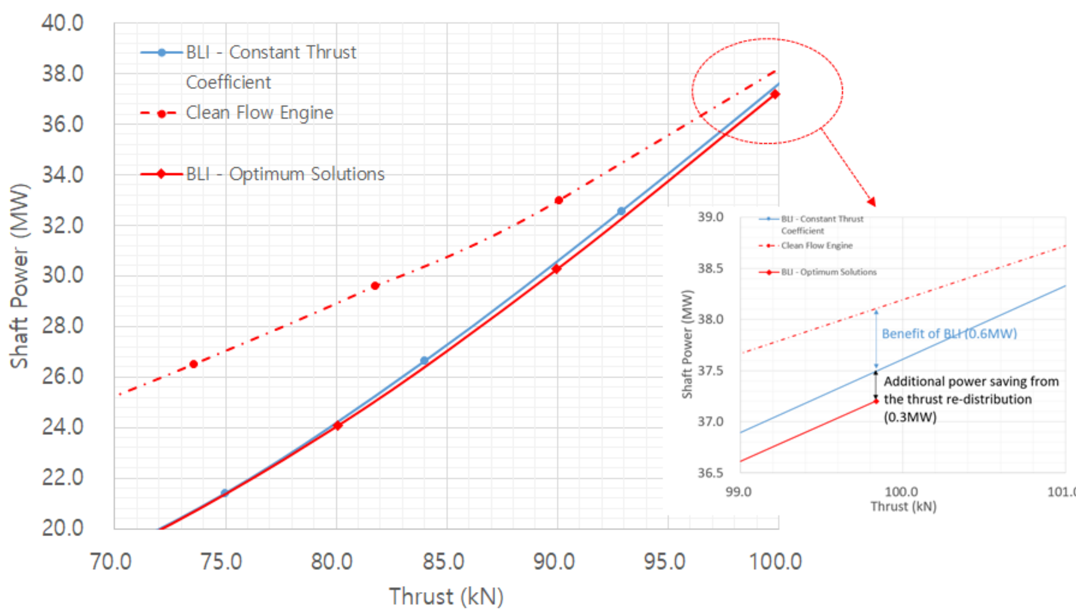

Figure 18. Shaft Power vs Thrust Curve after re-distribution of thrust at 16 slots.

Acknowledgement

In memory of the late Dr. Meng-Sing Liou, the authors sincerely appreciate and honor his passion and dedication to the development of the N3-X hybrid wing/body subsonic aircraft. We also appreciate financial support of NASA's AATT project and Mr. William Haller, the technical lead of the SA&I subproject. Special thanks to Dr. M.R. Mankbadi for inspiring the authors with an idea of the thrust sweep with actuator disk model with FUN3D CFD analyses through UPAI project.

References

[1] Felder, J., Kim, H. D., and Brown, G. V., "An Examination of the Effects of Boundary Layer Ingestion on Turboelectric Distributed Propulsion Systems," AIAA–2011–300, AIAA, 2011.

[2] Kim, H., Harding D., Gronstal, D., Liou, M.-F. and Liou, M.-S., "Design of the Hybrid Wing Body with Nacelle: N3-X Propulsion-Airframe Configuration" AIAA 2016-3875, 34th AIAA Applied Aerodynamics Conference, 13-17 June, 2016.

[3] Liou, M.-S., Kim, H. and Liou, M.-F., "Challenges and Progress in Aerodynamic Design of Hybrid Wingbody Aircraft with Embedded Engines," NASA/TM-2014-218309.

[4] Kim, H.J., and Liou, M.-S. "Flow simulation and optimal shape design of N3-X hybrid wing body configuration using a body force method," Aerospace Science and Technology, Vol. 71, pp. 661-674, Oct., 2017.

[5] Kim, H., Liou, M.-F. and Liou, M.-S. "Mail-Slot Nacelle Shape Design for N3-X Hybrid Wing Body Configuration," AIAA 2015-3805, AIAA Propulsion & Energy Forum 2015, Orlando, FL, 27-29 July 2015.

[6] Liou, M.-F., Kim, H.J., B.J.Lee, and Liou, M.S., "Aerodynamic Design of Integrated Propulsion-Airframe Configuration of the Hybrid Wingbody Aircraft," AIAA 2017-3411, 35th AIAA Applied Aerodynamics Conference, June 05-09, 2017, Denver, Co, 10.2514/6.2017-3411

[7] Hughes, C. E., "Aerodynamic Performance of Scale-Model Turbofan Outlet Guide Vanes Designed for Low Noise," AIAA-2002-0374, AIAA, 2002. Also NASA/TM-2001-211352, 2011.

[8] Liou, M.-S. And Lee, B. J., "Minimizing Inlet Distortion for Hybrid Wing Body Aircraft," J. Turbomachinery, 134, May 2012.

[9] Chima, R. V., "Rapid Calculations of Three-Dimensional Inlet/Fan Interaction," NASA Fundamental Aeronautics 2007 Annual Meeting, New Orleans, LA, Oct. 30–Nov. 1, 2007.

[10] Gray, J. S., Mader, C. A., Kenway, G. K.W., Martins, Joaquim R. R. A. "Approach to Modeling Boundary Layer Ingestion using a Fully Coupled Propulsion-RANS Model," AIAA-2017-1753, 58th AIAA/ASCE/AHS/ASC Structures, Structural Dynamics, and Materials Conference, AIAA SciTech Forum.

[11] Smith, L. H., "Wake Ingestion Propulsion Benefit," J. Propulsion and Power, Vol. 9, 74-82, 1993.

[12] FUN3D Manual V12.7, NASA TM-2015-218761, May 2017.

[13] Ordaz, I., Rallabhandi, S. K., Nielsen, E. J., and Diskin, B., "Mitigation of Engine Inlet Distortion through Adjoint-Based Design", AIAA 2017-3410, 35th AIAA Applied Aerodynamics Conference, June 05-09, 2017, Denver, Co.

[14] Jeong, S., Murayama, M., and Yamamoto, K., "Efficient Optimization Design Method Using Kriging Model, " J. of Aircraft, Vol. 42, No. 2, March-April 2005.

[15] Yim, J., Lee, B. J. and Kim, C. , "Exploring Multi-Stage Shape Optimization Strategy of Multi-Body Geometries Using Kriging-Based Model and Adjoint Method, " Computers & Fluids 68: 71 – 87, September 2012. 10.1016/j.compfluid.2012.07.015

[16] Deb, K. Agrawal, S., Pratap, A., Meyarivan, T., "A Fast and Elitist multi-objective Genetic Algorithm: NSGA-II," IEEE Transactions on Evolutionary Computation (IEEE-TEC), Vol.6, No.2, pp.182-197, 2002.